CMOS THz Camera Used as Compact Antenna Test Range

Robin Zatta, Vishal S. Jagtap, Janusz Grzyb, Ullrich R. Pfeiffer

2020 Third International Workshop on Mobile Terahertz Systems (IWMTS).
https://doi.org/10.1109/IWMTS49292.2020.9166379

CMOS THz Camera Used as Compact Antenna Test Range

Robin Zatta, Vishal S. Jagtap, Janusz Grzyb, and Ullrich R. Pfeiffer
Institute for High-Frequency and Communication Technology, University of Wuppertal, Germany
Email: zatta@uni-wuppertal.de

***Abstract*—In this paper, a silicon lens-integrated CMOS THz camera is employed as a compact antenna test range. The far-field radiation pattern of a 26-dBi 0.852-THz standard gain horn antenna radiation source is characterized. Both single-frame low-resolution and multi-frame super-resolution acquisition are performed. The latter is employed to measure a far-field radiation pattern with enhanced angular resolution. The directivity of the source is determined from both measured single-frame low-resolution and multi-frame super-resolution radiation patterns. The maximum directivity in the respective radiation patterns is 25 dBi and 25.8 dBi, respectively, determined with an accuracy of 1 dB and 0.2 dB. Improved accuracy in the latter is due to better angular resolution.**

***Index Terms*—Terahertz (THz), CMOS camera, compact antenna test range (CATR), far-field radiation pattern, geometrical multi-frame super-resolution.**

I. Introduction

In THz active imaging, it is essential to know the beam properties of the illumination source, such as shape, profile, and directivity, so that the beam artifacts can be distinguished from the object under illumination. Therefore, measuring radiation patterns of a source is indispensable. However, far-field radiation pattern characterization at a conventional far-field range is, in many cases, impractical or impossible [1]. Antennas being large in terms of wavelength develop their far-field radiation characteristic at a large distance from the antenna under test. This influences the far-field radiation pattern measurement capabilities significantly. Huge anechoic chambers would be required to carry out far-field measurements within controlled indoor facilities [2]. The far-field region of an antenna can be assumed to hold for distances greater than $2D^2/\lambda$ [3], where D is the diameter of a minimum sphere enclosing the antenna under test completely and λ the free-space wavelength. An alternative approach is to measure near-field radiation patterns, out of which far-field radiation patterns can be derived with the so-called near-to-far-field transformation [4]. Compared to radiation pattern measurements performed at a conventional far-field range, such performed in the near-field of an antenna under test are way easier to carry out. Unlike far-field characterization, the near-field characterization does not suffer from low SNR. Moreover, such near-field measurements can be performed in a rather compact manner. One specific approach deals with the so-called compact antenna test ranges; measurements are performed at a compact range, as the terminology implies. In such systems, a feed antenna is placed in the focal point of a collimator, such as a reflector [4] or a dielectric lens [5], to create an incident plane wave near the antenna under test. The chief advantage of a compact antenna test range is its small size.

Several applications of CMOS THz cameras have been demonstrated in recent years, such as THz active imaging [6]–[10], THz power metering [11], THz light-field imaging [12], object feature extraction with focused THz plenoptic imaging [13], [14], THz spectral analysis [15], and THz beam monitoring [16]. Most recently, THz super-resolution imaging using a CMOS THz camera has been demonstrated [17]. However, highly accurate far-field radiation pattern characterization of unknown THz sources has not been addressed within the application space of such measurement instruments. A few of the aforementioned applications need to be combined to make this possible. For example, unlike beam monitoring, radiation pattern characterization requires a measurement instrument with a high angular resolution, not only to extract directivity with high accuracy. According to [17], a CMOS THz camera can always reach maximum achievable angular resolution across the frequency and the full-frame with the help of geometrical multi-frame super-resolution techniques.

In this paper, we employ a commercially available hyper-hemispherical high-resistivity floating-zone silicon (HRFZ-Si) lens-integrated CMOS THz camera from Ticwave GmbH, Germany, Wuppertal, as a compact antenna test range to characterize the far-field radiation pattern of a 26-dBi 0.852-THz standard gain horn antenna radiation source. Both single-frame low-resolution and multi-frame super-resolution acquisition are performed. With a geometrical multi-frame super-resolution technique, it is ensured that the camera reaches its maximum achievable angular resolution across the full-frame, aiming at highly accurate directivity determination. Directivity extracted from far-field radiation patterns measured by both single-frame low-resolution and multi-frame super-resolution acquisition is compared. The maximum directivity extracted from the super-resolution far-field radiation pattern of the source is determined with an accuracy of 0.2 dB, calculated as the ratio of peak radiated power and overall radiated power; a single-frame low-resolution far-field radiation pattern goes along with an accuracy of 1 dB. Multi-frame acquisition has proven to substantially improve the accuracy in determining the directivity of an antenna under test due to enhanced angular resolution.

The outline of this paper is as follows. In Sec. II, it is

978-1-5386-5541-2/18/$31.00 ©2020 IEEE

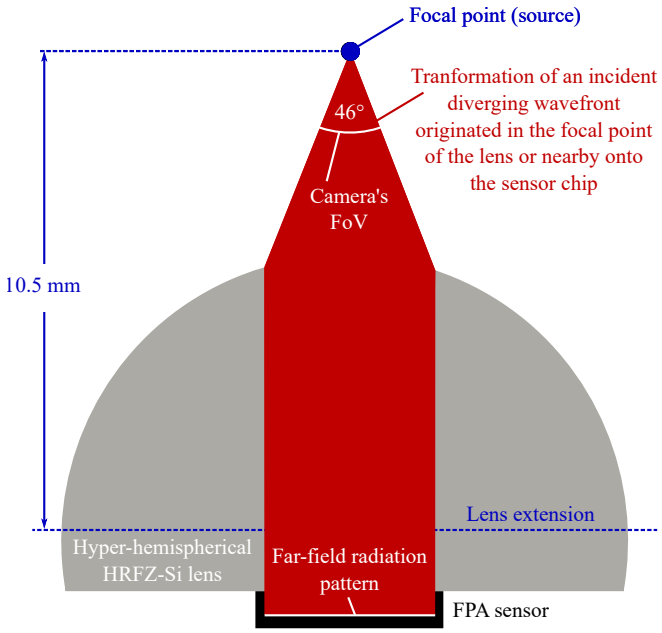

Figure 1. Illustration of how the camera can be used as a compact antenna test range. The camera's objective lens collimates a diverging incident wavefront of a radiation source placed in its focal point. This collimated beam then hits the FPA sensor surface, whereas each pixel receives radiation from a different angle [12]. As such, the near-field radiation pattern of a THz radiation source gets transformed into its far-field radiation pattern, which is then sampled by the camera's FPA sensor.

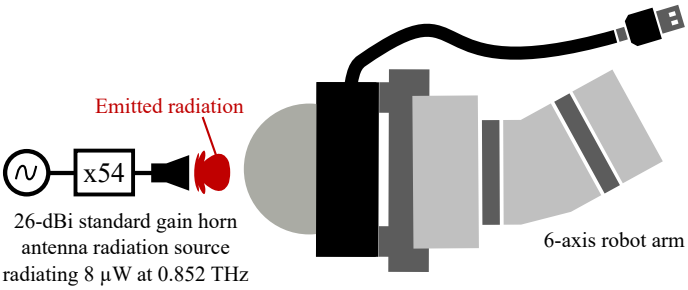

CMOS THz camera with video-rate optical NEP of 22 nW at 0.852 THz [9]; here, optical NEP about 687.5 pW (1024-frame averging)

Figure 2. Illustration of the experimental setup. For the proof of concept, the far-field radiation pattern of a standard gain horn antenna 0.6–1.1 THz radiation source is analyzed. The source is placed in the focal point of the camera's objective lens. The source was fixed, and the camera was mounted onto a 6-axis table-top robot arm for three-dimensional scanning. 4x4 low-resolution frames were acquired. Each frame corresponds to a single-frame low-resolution far-field radiation pattern. Superimposing all 4x4 acquired frames corresponds to a multi-frame super-resolution far-field radiation pattern. An improved angular resolution of the camera by super-resolution acquisition is aiming at improving the accuracy in extracting the source directivity.

explained how a hyper-hemispherical HRFZ-Si lens-integrated CMOS THz camera can be employed as a compact antenna test range, and its features that are relevant to this end are discussed. After that, Sec. III presents the measured far-field radiation patterns. Conclusions are drawn in Sec. IV.

II. CMOS THz Camera

The herein employed 5x5x3-cm^3 large hyper-hemispherical HRFZ-Si lens-integrated CMOS THz camera consists of a 32x32-pixel focal plane array (FPA) sensor of incoherently operated direct detectors. The FPA sensor adheres to the base of a 15-mm diameter hyper-hemispherical HRFZ-Si lens. Unlike operating the FPA sensor without any lens, the integration with the lens leads to an increased field-of-view (FoV), thereby improving the angular resolution of the individual camera pixels. The camera exhibits an FoV of 46°, mostly determined by the dimensions of its objective lens and FPA sensor. Frequency-dependent angular resolution limits of the camera have been discussed in [17]. Peak detector optical noise equivalent power (NEP) of 17 nW is recorded at 0.822 THz [11].

In common compact antenna test ranges, as discussed in [4], [5], an incident plane wave is created near an antenna under test to characterize a receiver. In our case, this whole thing works the opposite way. Fig. 1 illustrates how the CMOS THz camera can be used as a compact antenna test range. The camera's objective lens collimates the near-field radiation pattern of a source, representing a diverging incident wavefront. This collimated beam then gets spread across the FPA sensor's surface. Each camera pixel, thereby, samples incident radiation from a different incident angle, according to [12]. In other words, the near-field radiation pattern of a THz radiation source gets transformed into its far-field radiation pattern by the camera's objective lens, which is then subsequently sampled by the camera's FPA sensor.

III. Experimental Setup and Measured Results

Fig. 2 illustrates the experimental setup to measure the far-field radiation pattern of the 0.852-THz 26-dBi standard gain horn antenna radiation source using the CMOS camera. A synthesizer feeds the source, and the camera is operated by USB. The source is fixed in the focal point of the camera's objective lens, whereas the camera is mounted onto a 6-axis robot arm to enable three-dimensional scanning for sensing side lobes along with the main lobe of the antenna under test. According to [4], the distance between source and camera lens must be larger than the reactive far-field distance. At the source operating frequency of 0.852 THz, it is 0.35 mm. The distance between range and test antenna is with 3 mm significantly higher. THz absorbers were used wherever possible to minimize the influence of stray radiation within the room scattered or reflected by surrounding metal objects.

At 0.852 THz, the source radiates 8 µW, and the camera exhibits a video-rate optical NEP of about 22 nW [11]. A frame averaging of 1024 frames was applied to further improve upon the camera's optical NEP to 22 nW/$\sqrt{1024}$ ≈687.5 pW [11]. This way, the SNR was about 34.5 dB, which aided to sense the side lobes of the antenna under test with as much accuracy as possible to realize highly accurate determination of directivity. It is noted that capturing side lobes of an antenna under test is crucial in determining its directivity precisely. Another important thing to this ed is to provide a high angular resolution. At frequencies where the camera's fixed beam separation angle between adjacent pixels is larger than their individual frequency-

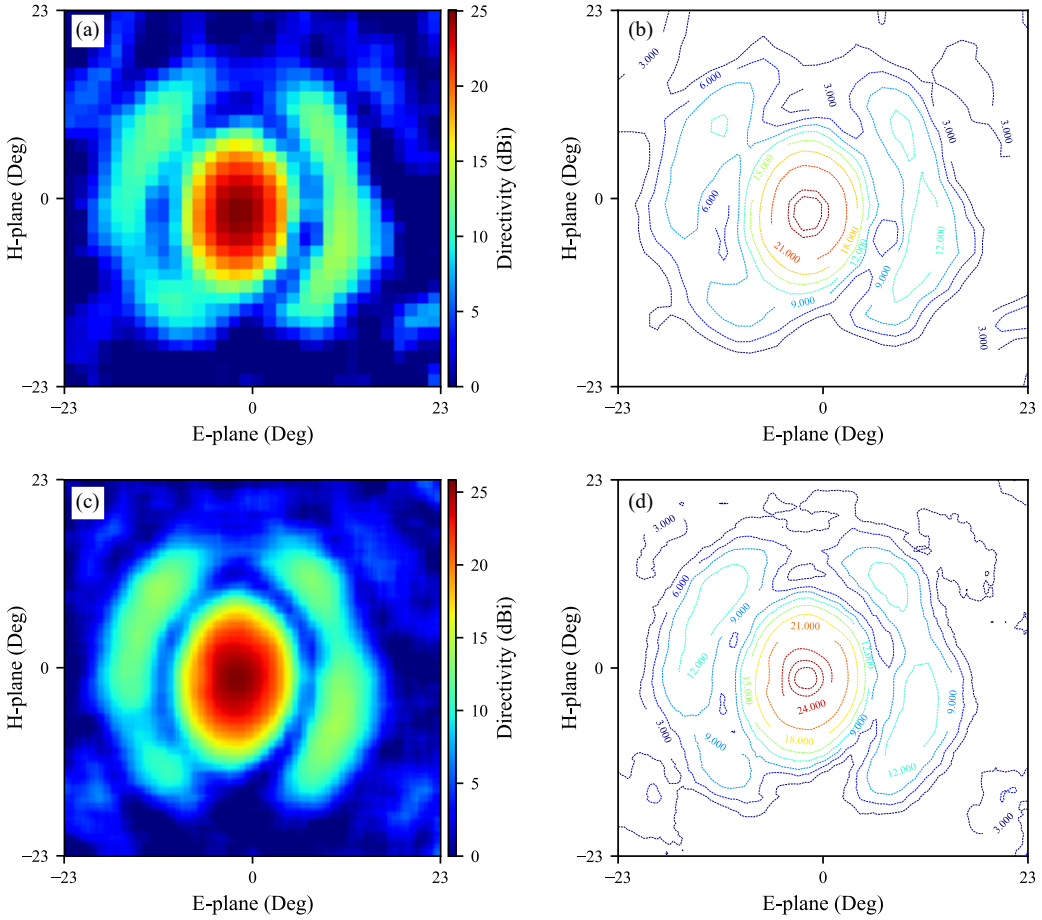

Figure 3. Results of far-field radiation patterns of a 26-dBi 0.852-THz radiation source measured with the here employed CMOS THz camera by both single-frame low-resolution and multi-frame super-resolution acquisition, shown in both image and contour plot representation in (a)–(b) and (c)–(d), respectively. In (a)/(b) and (c)/(d), the maximum directivity is 25 dBi and 25.8 dBi, respectively, determined with an accuracy of 1 dB and 0.2 dB.

dependent FWHM beam divergence angles that relate to their directivity, the camera under-samples its FoV. Geometrical multi-frame super-resolution techniques used for over-sampling are capable of overcoming this limitation. Here, multiple images are acquired at angular offsets and superimposed accordingly. According to [17], the camera can reach an angular resolution of 1.6° at the frequency of interest across the full-frame with such techniques.

To measure multiple (4x4) single-frame low-resolution far-field radiation patterns at angular offsets, which may be superimposed into a multi-frame super-resolution radiation pattern, a two-dimensional goniometric scan around the center of the camera's objective lens was performed. The opening angle was as large as the beam separation angle between two adjacent camera pixels, i.e., 1.6°, and the angular resolution was 0.4° in both theta and phi. This way, under-sampled areas between pixel pairs can be "filled" when superimposing the single-frames. The camera's fixed pattern noise was removed at the beginning of the measurement. Therefore and because of averaging across 1024 frames per low-resolution far-field radiation pattern, the total measurement time was about 8.5 minutes. It is noted that none of the camera pixels was saturated at any point in time, which would cause a systematic error in determining the directivity.

Measured low-resolution far-field radiation patterns were processed with the super-resolution algorithm described in [17]. As a result, a super-resolution far-field radiation pattern was generated. This one provides enhanced angular resolution. To reduce the effect of standing waves, measured far-field radiation patterns were convoluted with carefully selected two-dimensional Gaussian kernels; such convolution works similarly to notch filtering applied in [18], used to deal with standing waves from measured data. In single-frame low-resolution and multi-frame super-resolution far-field radiation patterns, Gaussian kernels of 3x3 and 9x9 elements have been applied, respectively.

Fig. 3 shows the measured results. Single-frame low-resolution and multi-frame super-resolution far-field radiation patterns are shown in both image plot and contour plot representation in (a)/(c) and (b)/(d), respectively. The low-resolution far-field radiation pattern represents one acquired frame. The far-field radiation pattern acquired by multi-frame super-resolution, on the other hand, contains information from 4x4 frames acquired. In both cases, the directivity is calculated

as the ratio of radiated power per angular position divided by the integral of the overall radiated power across the entire far-field radiation pattern, normalized to the camera's beam separation angle, which is smaller by a factor of four in the superimposed multi-frame super-resolution far-field radiation pattern. As such, the directivity at each angular position is determined. It is noted that backside radiation is neglected in the calculations. The maximum directivity extracted from both low-resolution and super-resolution far-field radiation patterns is 25 dBi and 25.8 dBi, respectively. Hence, the corresponding error is 1 dB and 0.2 dB, respectively, considering the source manual giving us the directivity to be 26 dBi at 0.852 THz. Moreover, directivity is calculated using an average Full-Width at Half-Maximum (FWHM) beam divergence angle across both E-plane and H-plane. In the low-resolution and super-resolution far-field radiation pattern, this averaged angle is 8.45° and 8.62°, respectively. According to [19], the directivity of an antenna can be calculated as $D_{dBi}=10\cdot\log_{10}(32400/\theta^2)$, where θ denotes the FWHM beam divergence angle. Based on that, the maximum directivity is 26.6 dBi and 26.4 dBi, respectively. Here, the error is 0.6 dB and 0.4 dB, respectively. Since this relation is only true for antennas with neglectable side lobes, the directivity is slightly overestimated. This minor deviation, however, also proves that the source was placed in the focal point of the camera or nearby since this kind of directivity extraction procedure is not a relative one, but it is based on an absolute measure.

IV. Conclusions and Perspectives

In this paper, a CMOS THz camera has been employed as a compact antenna test range. For demonstration purposes, the far-field radiation pattern of a 26-dBi 0.852-THz standard gain horn antenna radiation source has been characterized. Single-frame low-resolution and multi-frame super-resolution acquisition were performed. The latter was employed to enhance the angular resolution of the camera. Directivity of the antenna under test has been extracted from both low-resolution and super-resolution far-field radiation patterns, with a maximum directivity of 25 dBi and 25.8 dBi, respectively. The corresponding error is 1 dB and 0.2 dB, respectively, in which super-resolution acquisition resulted in an even more accurate determination of directivity due to an improved angular resolution of the employed camera.

Measuring far-field radiation patterns of a THz radiation source at a compact range with a CMOS THz camera substantially improves upon the data acquisition time. However, one limitation needs to be considered: main as well as side lobes of an antenna under test need to be captured to determine its directivity appropriately. For this reason, the presented method works better for highly directive sources. Capturing different parts of a source's radiation pattern by performing a goniometric scan around an antenna under test may overcome this limitation.

In future work, the compact antenna test range based on hyper-hemispherical HRFZ-Si lens-integrated CMOS THz camera needs to be analyzed in the following problem areas: pixel-to-pixel variation, diffraction from lens edges, depolarization, the interaction between range and test antenna, lens surface tolerances, and stray radiation within the room.

Acknowledgements

The authors would like to thank Ticwave GmbH, Germany, for providing the camera module. This work was partially funded by the DFG SFB/TRR 196 MARIE under project C08.

References

[1] D. T. Paris and F. K. Hurd, *Basic electromagnetic theory*. McGraw-Hill Companies, 1969.

[2] T. Zwick, C. Baks, U. R. Pfeiffer, Duixian Liu, and B. P. Gaucher, "Probe based MMW antenna measurement setup," in *IEEE Antennas and Propagation Society Symposium, 2004.*, vol. 1, June 2004, pp. 747–750 Vol.1.

[3] S. Silver, *Microwave antenna theory and design*. Iet, 1984, no. 19.

[4] R. C. Johnson, H. A. Ecker, and J. S. Hollis, "Determination of far-field antenna patterns from near-field measurements," *Proceedings of the IEEE*, vol. 61, no. 12, pp. 1668–1694, 1973.

[5] J. R. Mentzer, "The use of dielectric lenses in reflection measurements," *Proceedings of the IRE*, vol. 41, no. 2, pp. 252–256, 1953.

[6] R. Al Hadi *et al.*, "A 1 k-pixel video camera for 0.7–1.1 terahertz imaging applications in 65-nm cmos," *IEEE Journal of Solid-State Circuits*, vol. 47, no. 12, pp. 2999–3012, 2012.

[7] S. Malz, R. Jain, and U. R. Pfeiffer, "Towards passive imaging with CMOS THz cameras," in *2016 41st International Conference on Infrared, Millimeter, and Terahertz waves (IRMMW-THz)*, Sep. 2016, pp. 1–2.

[8] D. Headland, R. Zatta, and U. R. Pfeiffer, "Diffuse Beam with Electronic THz Source Array," in *2018 43rd International Conference on Infrared, Millimeter, and Terahertz Waves (IRMMW-THz)*, Sep. 2018, pp. 1–2.

[9] P. Hillger, J. Grzyb, R. Jain, and U. R. Pfeiffer, "Terahertz Imaging and Sensing Applications With Silicon-Based Technologies," *IEEE Transactions on Terahertz Science and Technology*, vol. 9, no. 1, pp. 1–19, Jan 2019.

[10] R. Zatta, R. Jain, D. Headland, and U. R. Pfeiffer, "Incoherent power combining of thz source arrays," in *2019 44th International Conference on Infrared, Millimeter, and Terahertz Waves (IRMMW-THz)*, 2019, pp. 1–2.

[11] R. Zatta, R. Jain, and U. R. Pfeiffer, "Characterization of the noise behavior in lens-integrated CMOS terahertz video cameras," *Terahertz Sicience and Technology - The International Journal of THz*, vol. 11, no. 4, pp. 102–123, Dec. 2018.

[12] R. Jain, J. Grzyb, and U. R. Pfeiffer, "Terahertz light-field imaging," *IEEE Transactions on Terahertz Science and Technology*, vol. 6, no. 5, pp. 649–657, 2016.

[13] R. Jain, F. Landskron, J. Grzyb, and U. R. Pfeiffer, "Object Feature Extraction with Focused Terahertz Plenoptic Imaging," in *2018 43rd International Conference on Infrared, Millimeter, and Terahertz Waves (IRMMW-THz)*. IEEE, 2018, pp. 1–2.

[14] R. Jain, M. Schellenbeck, J. Grzyb, and U. R. Pfeiffer, "Investigations on the plenoptics based image generation for THz reflection imaging," in *2017 42nd International Conference on Infrared, Millimeter, and Terahertz Waves (IRMMW-THz)*, Aug 2017, pp. 1–2.

[15] D. Headland, P. Hillger, R. Zatta, and U. Pfeiffer, "Incoherent, spatially-mapped THz spectral analysis," in *2018 43rd International Conference on Infrared, Millimeter, and Terahertz Waves (IRMMW-THz)*, Sep. 2018, pp. 1–2.

[16] R. Al Hadi, J.-F. Lampin, and U. R. Pfeiffer, "A real-time terahertz beam monitoring application with a 1024-pixel CMOS terahertz camera module," in *CLEO: Applications and Technology*. Optical Society of America, 2014, pp. JTu4A–107.

[17] R. Zatta, R. Jain, J. Grzyb, and U. R. Pfeiffer, "Resolution Limits in Lens-Integrated CMOS THz Cameras Employing Super-Resolution Imaging," in *2019 44th International Conference on Infrared, Millimeter, and Terahertz Waves (IRMMW-THz)*, Sep. 2019, pp. 1–2.

[18] V. S. Jagtap, R. Zatta, J. Grzyb, and U. R. Pfeiffer, "Performance Characterization Method of Broadband Terahertz Video Cameras," in *2019 44th International Conference on Infrared, Millimeter, and Terahertz Waves (IRMMW-THz)*, Sep. 2019, pp. 1–2.

[19] C. A. Balanis, *Antenna theory: analysis and design*. John wiley & sons, 2016.